

Efficiently Adversarial Examples Generation for Visual-Language Models under Targeted Transfer Scenarios using Diffusion Models

Qi Guo

Xi'an Jiaotong University
Xi'an, China
gq19990314@stu.xjtu.edu.cn

Xiaojun Jia

Nanyang Technological University
Singapore, Singapore
jiaxiaojunqiang@gmail.com

Shanmin Pang

Xi'an Jiaotong University
Xi'an, China
pangsm@xjtu.edu.cn

Qing Guo

Center for Frontier AI Research
Singapore, Singapore
tsingqguo@ieee.org

ABSTRACT

Targeted transfer-based attacks involving adversarial examples pose a significant threat to large visual-language models (VLMs). However, the state-of-the-art (SOTA) transfer-based attacks incur high costs due to excessive iteration counts. Furthermore, the generated adversarial examples exhibit pronounced adversarial noise and demonstrate limited efficacy in evading defense methods such as DiffPure. To address these issues, inspired by score matching, we introduce AdvDiffVLM, which utilizes diffusion models to generate natural, unrestricted adversarial examples. Specifically, AdvDiffVLM employs Adaptive Ensemble Gradient Estimation to modify the score during the diffusion model's reverse generation process, ensuring the adversarial examples produced contain natural adversarial semantics and thus possess enhanced transferability. Simultaneously, to enhance the quality of adversarial examples further, we employ the GradCAM-guided Mask method to disperse adversarial semantics throughout the image, rather than concentrating them in a specific area. Experimental results demonstrate that our method achieves a speedup ranging from 10X to 30X compared to existing transfer-based attack methods, while maintaining superior quality of adversarial examples. Additionally, the generated adversarial examples possess strong transferability and exhibit increased robustness against adversarial defense methods. Notably, AdvDiffVLM can successfully attack commercial VLMs, including GPT-4V, in a black-box manner.

CCS CONCEPTS

• Security and privacy → Human and societal aspects of security and privacy.

KEYWORDS

Adversarial Examples, Visual-Language Models, Diffusion Models

1 INTRODUCTION

Large VLMs have demonstrated significant success in tasks such as image-to-text generation [12–14] and text-to-image generation [2, 21]. Particularly in image-to-text generation, users can use images to generate executable commands for robot control, with potential applications in autonomous driving systems, assistance systems for the visually impaired, and content moderation systems. Errors in these applications can lead to severe security risks, jeopardizing

the lives and property of individuals. Consequently, it is crucial to assess the adversarial robustness of these VLMs.

Recent studies [1, 11] have explored the adversarial robustness of VLMs, primarily focusing on untargeted and white-box scenarios. However, the more realistic settings of black-box and targeted scenarios have not received adequate attention. AttackVLM [31] employs a query-based attack method and incorporates transfer-based priors to prompt black-box VLMs to produce targeted responses. However, due to the substantial number of queries required, this process is time-consuming, typically requiring several hours to generate an adversarial example. Consequently, we consider an alternative black-box attack method, namely, transfer-based attacks. As shown in Figure 1, the current SOTA transfer-based attacks are also slow in generating adversarial examples and less effective in evading adversarial defense methods. Additionally, the adversarial examples generated by these methods exhibit significant noise.

To address these problems, inspired by score matching [26] and unrestricted adversarial examples [25], we propose AdvDiffVLM that uses diffusion models to generate natural unrestricted adversarial examples. Specifically, we leverage and modify the reverse generation process of the pre-trained diffusion models, where we utilize Adaptive Ensemble Gradient Estimation to change score and embed target semantics into adversarial examples. To enhance the naturalness of the output, we introduce the GradCAM-guided Mask, which disperses the adversarial target semantics across adversarial examples, preventing the model from generating adversarial examples in specific areas and thereby improving image quality. Our method requires only a few steps of backward denoising to generate adversarial examples, making it significantly faster than current transfer-based methods. Furthermore, AdvDiffVLM generates adversarial examples through denoising, exhibiting greater robustness to defense methods.

We summarize our contributions as follows: **1)** We provide a comprehensive evaluation of the robustness of VLMs against the SOTA transfer-based attacks in targeted and transfer scenarios; **2)** We introduce AdvDiffVLM, which utilizes Adaptive Ensemble Gradient Estimation and the GradCAM-guided Mask to produce natural, unrestricted adversarial examples; **3)** Experimental results demonstrate that AdvDiffVLM achieves speedups of an order of magnitude or greater over previously published attackers, while delivering adversarial examples with superior image quality. Moreover, these adversarial examples exhibit robust transferability across

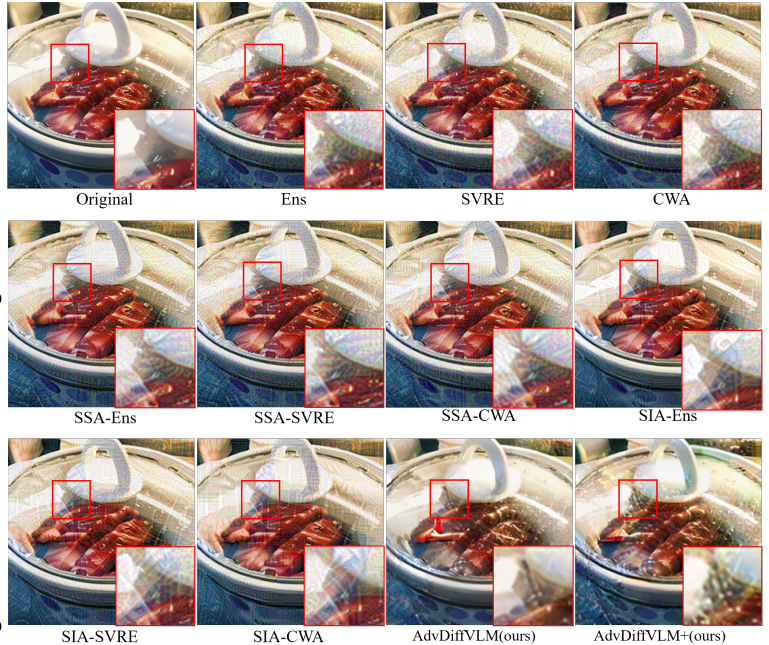
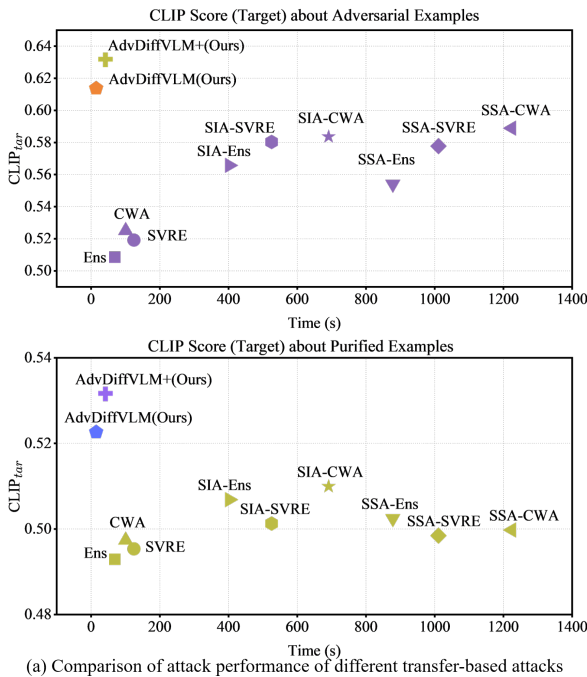


Figure 1: Comparison of different transfer-based attacks and our method on VLMs. (a) Comparison of attack performance. We select BLIP2 [12] as the representation model of VLMs. We report the $CLIP_{tar}$ score, which is the similarity between the response generated by the input images (Adversarial Examples or Purified Examples) and the pre-defined adversarial target texts (see Appendix 4.3 for specific calculation methods). Purified Examples represent the adversarial examples purified by DiffPure [19]. **(b) Comparison of image quality.** We enlarge the local area of the adversarial examples to enhance visual effects. It is evident that adversarial examples generated by transfer-based attacks exhibit notable noise. Our method has better visual effects. Magnify images for improved contrast.

VLMs and significant robustness against defense methods; 4) Our method can successfully attack commercial VLMs such as GPT-4V in black-box scenarios (<https://chat.openai.com/>).

2 RELATED WORKS

2.1 Adversarial Attacks in VLMs

Adversarial attack methods are categorized into white-box and black-box attacks based on adversary knowledge, and into targeted and untargeted attacks based on adversary goals. There have been studies examining the robustness of VLMs, specifically addressing adversarial challenges in visual question answering [31] and image captioning [1]. However, most investigations focus on traditional CNN-RNN-based models, with assumptions of either white-box access or untargeted goals, limiting their applicability in real-world scenarios. Recently, AttackVLM [31] implemented both transfer-based and query-based attacks on large open-source VLMs, under the assumption of black-box access and targeted goals. Nevertheless, this approach is time-intensive, owing to its dependence on numerous VLM queries. Additionally, [6] investigated VLM adversarial robustness via ensemble transfer-based attacks, albeit assuming untargeted goals. In this study, we explore the adversarial robustness of VLMs under targeted transfer-based attacks. Initially, we assess VLMs robustness against current SOTA transfer-based attacks, in

conjunction with AttackVLM. Subsequently, we analyze the limitations of current methods and implement targeted improvements, culminating in the proposal of AdvDiffVLM.

2.2 Unrestricted Adversarial Examples

Due to the inadequacy of the l_p norm distance in capturing human perception, there has been increasing interest among researchers in unrestricted adversarial examples in recent years. Some approaches employ generative methods to generate unrestricted adversarial examples. For instance, [25, 32] perturbed the latent representation of GANs to generate unrestricted adversarial examples. However, due to the limited interpretability of GANs, the generated adversarial examples exhibit poor quality. Diffusion models [10] are SOTA generative models based on likelihood with theoretical foundations, sampling data distribution with high fidelity and diversity. AdvDiffuser [5] integrated the PGD [17] method into the reverse process of the diffusion model, yielding high-quality unrestricted adversarial examples. In this study, we explore using the diffusion model for generating unrestricted adversarial examples, focusing on modifying the score in the diffusion model’s inverse process rather than adding noise to the latent image.

More details for diffusion models are described in Appendix 2 and the code is available in (Supplementary Material).

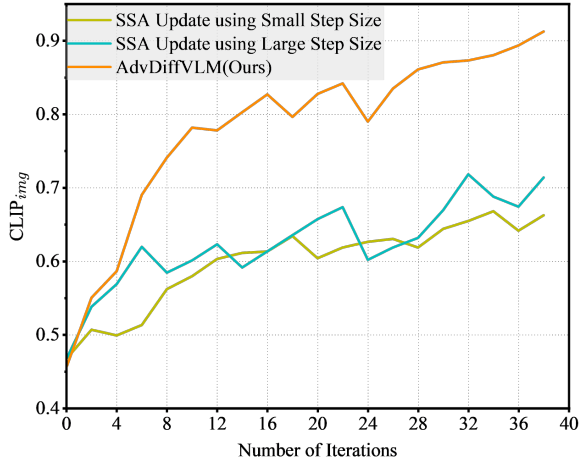


Figure 2: The CLIP_{img} score varies with the number of iterations, where CLIP_{img} is the similarity between the adversarial examples and the adversarial target images, which is calculated by the visual encoder of CLIP ViT-B/32. We choose SSA [15] as the representative of transfer-based attacks.

3 PRELIMINARIES

3.1 Problem Settings

We denote the victim VLM model as f_{ξ} , and aim to induce f_{ξ} to output the target response. This can be formalized as

$$\begin{aligned} \max CS(g_{\psi}(f_{\xi}(\mathbf{x}_{adv}; \mathbf{c}_{in})), g_{\psi}(\mathbf{c}_{tar})) \\ \text{s.t. } D(\mathbf{x}, \mathbf{x}_{adv}) \leq \delta \end{aligned} \quad (1)$$

where $\mathbf{x} \in \mathbb{R}^{3 \times H \times W}$ represents the original image, \mathbf{x}_{adv} and \mathbf{c}_{tar} respectively refer to adversarial example and adversarial target text, and $g_{\psi}(\cdot)$ denotes the CLIP text encoder. Besides, $D(\mathbf{x}, \mathbf{x}_{adv}) \leq \delta$ places a bound on a distance metric, and $CS(\cdot, \cdot)$ refers to the cosine similarity metric. Finally, \mathbf{c}_{in} and \mathbf{c}_{out} denote the input text and the output text, respectively.

Since f_{ξ} is a black-box model, we generate adversarial examples on the surrogate model ϕ_{ψ} and subsequently transfers them to f_{ξ} . In addition, inspired by [31], matching image-image features can lead to better results, we define the problem as,

$$\begin{aligned} \max CS(\phi_{\psi}(\mathbf{x}_{adv}), \phi_{\psi}(\mathbf{x}_{tar})) \\ \text{s.t. } D(\mathbf{x}, \mathbf{x}_{adv}) \leq \delta \end{aligned} \quad (2)$$

where \mathbf{x}_{tar} represents the target image generated by \mathbf{c}_{tar} . We use stable diffusion [21] to implement the text-to-image generation. ϕ_{ψ} refers to CLIP image encoder. Our study is the most realistic and challenging attack scenarios, i.e., targeted and transfer scenarios.

3.2 Rethinking Transfer-based Attacks

Transfer-based attacks can effectively solve Eq.2. In this context, we assess the robustness of VLMs against current SOTA transfer-based attacks, in conjunction with AttackVLM. Specifically, we consider ensemble attacks such as Ens[7], SVRE [29], and CWA [4], as well as data augmentation attacks like SSA [15] and SIA [27], and combinations of these techniques. We primarily employ the simple ensemble version of data augmentation attacks, as relying on a

single surrogate model tends to yield poor performance. A detailed introduction to these methods, along with their hyper-parameter settings, is provided in Appendix 4.2.

The outcomes of these transfer-based attacks on VLMs are depicted in Figure 1. As illustrated in Figure 1, current transfer-based attacks face challenges such as slow adversarial example generation, noticeable noise within these examples, and limited capability to evade adversarial defense methods. The limitations of existing transfer-based attacks on VLMs are analyzed as follows: First, existing SOTA transfer-based attacks only access the original image during the optimization of Eq.2. Consequently, they employ small steps and strategies like data augmentation to tentatively approach the optimal solution, necessitating numerous iterations and resulting in high attack costs. As shown in Figure 2, using a larger step size results in pronounced fluctuations during the optimization process. This issue may be mitigated by leveraging score, which provides insights into the data distribution. By offering score guidance towards solving Eq.2, quicker convergence is expected. Therefore score information can be considered in the design of new improved attack method. Second, existing transfer-based attacks introduce high-frequency additive noise, which can be readily countered by adversarial defense methods. Unrestricted adversarial examples [23] have proven effective at bypassing defense methods, suggesting that new transfer-based attacks could adopt this approach.

4 METHODOLOGY

In this section, we present adversarial attacks from the perspective of score matching and then offer a comprehensive description of the proposed AdvDiffVLM. Finally, we delineate the distinctions between our method and AdvDiffuser. The complete workflow chart of AdvDiffVLM is illustrated in Figure 3.

4.1 Theoretical Background

We are focused on modeling adversarial attacks from a generative perspective, considering how to utilize the data distribution (score) of the generative model to generate natural, unrestricted adversarial examples. Additionally, as indicated in [16], learning to model the score function is equivalent to modeling the negative of the noise, suggesting that score matching and denoising are equivalent processes. Thus, our method derives from integrating diffusion models and score matching, positioning it as a novel approach for generating high-quality, unrestricted adversarial examples.

Formally, we want to obtain distribution meeting the condition that the adversarial example has target semantic information during the reverse generation process

$$p(x_{t-1}|x_t, f_{\xi}(\mathbf{x}_{adv}; \mathbf{c}_{in})) = \mathbf{c}_{tar} \quad (3)$$

where x_t represents the latent image of the diffusion model. To the end, we start from the perspective of score matching [26] and consider the score $\nabla \log p(x_{t-1}|x_t, \mathbf{c}_{tar})$ of this distribution, where ∇ is the abbreviation for ∇_{x_t} . According to Bayes theorem (see

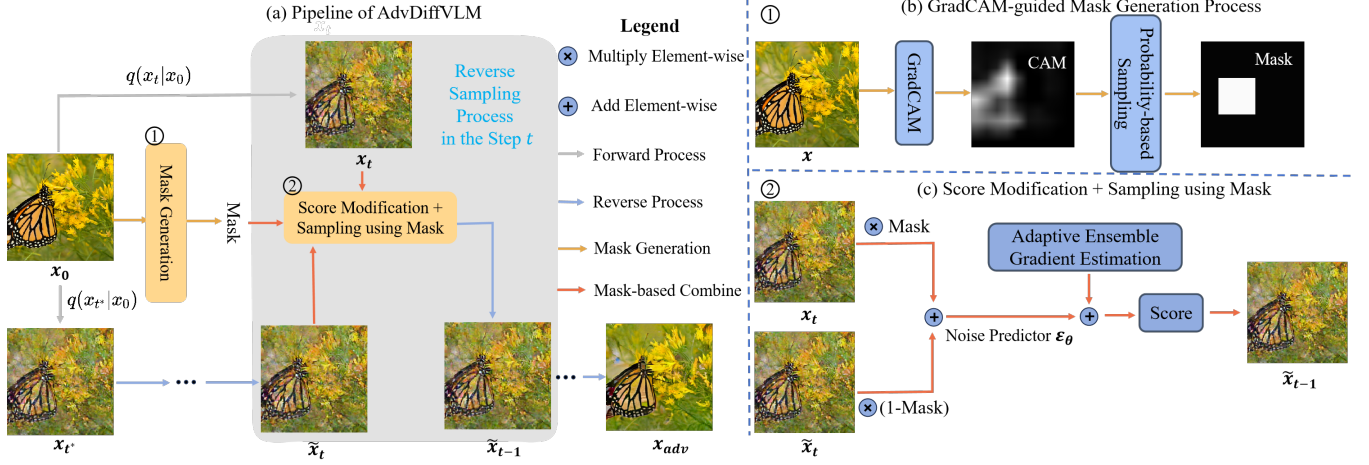


Figure 3: An overview of the AdvDiffVLM for efficiently generating transferable unrestricted adversarial examples. AdvDiffVLM mainly includes two components: Adaptive Ensemble Gradient Estimation and GradCAM-guided Mask. Details are respectively described in Secs. 4.2 and 4.3. Please refer to Section 4 for specific symbol meanings.

Appendix 3.1 for detailed explanations),

$$\begin{aligned}
\nabla \log p(x_{t-1} | x_t, c_{tar}) &= \nabla \log \left(\frac{p(c_{tar} | x_{t-1}, x_t) \cdot p(x_{t-1} | x_t)}{p(c_{tar} | x_t)} \right) \\
&= \nabla \log p(c_{tar} | x_{t-1}, x_t) + \nabla \log p(x_{t-1} | x_t) - \nabla \log p(c_{tar} | x_t) \\
&= \nabla \log p(c_{tar} | x_{t-1}) + \nabla \log p(x_t | x_{t-1}, c_{tar}) \\
&\quad - \nabla \log p(x_t | x_{t-1}) + \nabla \log p(x_{t-1} | x_t) - \nabla \log p(c_{tar} | x_t) \\
&= \nabla \log p(x_t | x_{t-1}, c_{tar}) - \nabla \log p(x_t | x_{t-1}) \\
&\quad + \nabla \log p(x_{t-1} | x_t) - \nabla \log p(c_{tar} | x_t)
\end{aligned} \tag{4}$$

$p(x_t | x_{t-1}, c_{tar})$ and $p(x_t | x_{t-1})$ respectively denote the add noise process with target text and the add noise process devoid of target semantics. From an intuitive standpoint, whether target text is present or not, the forward noise addition process follows a Gaussian distribution, and the added noise remains consistent, indicating that the gradient solely depends on x_t . The difference between x_t without target text and x_t with target text is minimal, as constraints are employed to ensure minimal variation of the adversarial sample from the original sample. Therefore, $\nabla \log p(x_t | x_{t-1}, c_{tar})$ and $\nabla \log p(x_t | x_{t-1})$ are approximately equal. So the final score is $\nabla \log p(x_{t-1} | x_t) - \nabla \log p(c_{tar} | x_t)$.

Because score matching and denoising are equivalent processes, that is, $\nabla \log p(x_t) = -\frac{1}{\sqrt{1-\alpha_t}} \epsilon_\theta$. Therefore we can get score $(\nabla \log p(x_{t-1} | x_t, c_{tar}))$,

$$\text{score} = -\left(\frac{\epsilon_\theta(x_t)}{\sqrt{1-\alpha_t}} + \nabla \log p_{f_\xi}(c_{tar} | x_t) \right) \tag{5}$$

Where ϵ_θ represents the noise predictor of the diffusion model, and $\bar{\alpha}_t$ represents the hyperparameters in the diffusion model.

Eq.5 demonstrates that the score of $p(x_{t-1} | x_t, c_{tar})$ can be derived by incorporating gradient information into the inverse process of the diffusion model. Consequently, adversarial semantics can be incrementally embedded into adversarial examples based on the principle of score matching.

4.2 Adaptive Ensemble Gradient Estimation

Since f_ξ is a black-box model and cannot obtain gradient information, we use surrogate model to estimate $\nabla \log p_{f_\xi}(c_{tar} | x_t)$. As a scalable method for learning joint representations between text and images, CLIP [20] can leverage pre-trained CLIP models to establish a bridge between images and text. Therefore we use the CLIP model as the surrogate model to estimate the gradient.

Specifically, we first add noise to the original image x by t^* steps through the forward process $q(x_{t^*} | x_0)$ to obtain x_{t^*} , where $x_0 = x$. Then, at each step of reverse process, we change score:

$$\text{score} = -\left(\frac{1}{\sqrt{1-\bar{\alpha}_t}} \epsilon_\theta(\tilde{x}_t) + s \nabla_{\tilde{x}_t} (CS(\phi_\psi(\tilde{x}_t), \phi_\psi(x_{tar}))) \right) \tag{6}$$

where s is the adversarial gradient scale used to control the degree of score change and \tilde{x}_t is the latent image in the inverse process.

We find that gradient estimation using only a single surrogate model is inaccurate. Therefore, we consider using a set of surrogate models $\{\phi_\psi^i\}_{i=1}^{N_m}$ to better estimate the gradient. Specifically, we make the following improvements to Eq. 6:

$$\text{score} = -\left(\frac{\epsilon_\theta(\tilde{x}_t)}{\sqrt{1-\bar{\alpha}_t}} + s \nabla_{\tilde{x}_t} (w_i \sum_{i=1}^{N_m} CS(\phi_\psi^i(\tilde{x}_t), \phi_\psi^i(x_{tar}))) \right) \tag{7}$$

where $\mathbf{w} = (w_1, w_2, \dots, w_{N_m})$ represents the weight of cosine loss of different models.

Since different images have different sensitivities to surrogate models, only using simple ensemble cannot obtain optimal solution. Inspired by [3] (see Appendix 3.2), we propose a new adaptive ensemble method, and obtain \mathbf{w} in Eq. 7 in the following way:

$$w_i(t) = \frac{\sum_{j=1}^{N_m} \exp(\tau \mathcal{L}_j(t+1) / \mathcal{L}_j(t+2))}{N_m \exp(\tau \mathcal{L}_i(t+1) / \mathcal{L}_i(t+2))} \tag{8}$$

where τ refers to the temperature. A larger τ makes all weights close to 1. $\mathcal{L}_i = CS(\phi_\psi^i(\tilde{x}_t), \phi_\psi^i(x_{tar}))$. We initialize $\{w_i(t^*)\}_{i=1}^{N_m}$ and $\{w_i(t^*-1)\}_{i=1}^{N_m}$ to 1. Through Eq. 8, we reduce the weight of surrogate models with fast-changing losses to ensure that gradient estimations of different surrogate models are updated simultaneously.

Algorithm 1 The overall algorithm of AdvDiffVLM

- 1: **Input:** original image \mathbf{x} , N_m surrogate models ϕ_{θ}^i , adversarial guidance scale s , reverse generation process timestep t^* , mask area size k , perturbation threshold ϵ , temperature τ , adversarial target image \mathbf{x}_{tar} .
 - 2: **Output:** adversarial example \mathbf{x}_{adv}
 - 3: Initialize $\{w_i\}_{i=1}^{N_m} = 1$, CAM, $x_0 = \mathbf{x}$;
 - 4: Sample $x_{t^*} \sim q(x_{t^*} | x_0)$, let $\tilde{x}_{t^*} = \tilde{x}_{t^*} = x_{t^*}$;
 - 5: **for** $t \leftarrow t^*, \dots, 1$ **do**
 - 6: Get mask m according to CAM;
 - 7: $x_t \sim q(x_t | x_0)$;
 - 8: $\hat{x}_t = m \odot x_t + (1 - m) \odot \tilde{x}_t$;
 - 9: $w_i = \frac{\sum_{j=1}^{N_m} \exp(\tau \mathcal{L}_j(t+1) / \mathcal{L}_j(t+2))}{N_m \exp(\tau \mathcal{L}_i(t+1) / \mathcal{L}_i(t+2))}$;
 - 10: $g = \nabla_{\tilde{x}_t} (w_i \sum_{i=1}^{N_m} CS(\phi_{\psi}^i(\tilde{x}_t), \phi_{\psi}^i(\mathbf{x}_{\text{tar}})))$;
 - 11: $g = \text{clip}(g, -\delta, \delta)$;
 - 12: $\text{score} = \epsilon_{\theta}(\hat{x}_t) / \sqrt{1 - \bar{\alpha}_t} + s \cdot g$;
 - 13: $\tilde{x}_{t-1} = -\sqrt{1 - \bar{\alpha}_t} \times \text{score}$;
 - 14: **end for**
 - 15: **Return:** $\mathbf{x}_{\text{adv}} = \tilde{x}_0$
-

Finally, we set the perturbation threshold δ , and then clip the adversarial gradient to ensure the naturalness of the synthesized adversarial examples.

4.3 GradCAM-guided Mask Generation

We detail Adaptive Ensemble Gradient Estimation in the previous section. However, we note that only relying on adaptive ensemble gradient estimation leads to the generation of obvious adversarial features in specific areas, resulting in poor visual effects. To achieve a balance between the natural visual effects and attack capabilities of adversarial examples, we introduce GradCAM-guided Mask. This method utilizes a mask to combine the forward noisy image x_t and the generated image \tilde{x}_t . Through the combination, the adversarial semantics concentrated in the adversarial examples across the entire image is distributed, thereby enhancing natural visual effect of the adversarial examples. We present the visualization results before and after adding GradCAM-guided Mask in Appendix 5.1.

First, we utilize GradCAM [22] to derive the class activation map CAM of \mathbf{x} with respect to ground-truth label \mathbf{y} . CAM assists in identifying important and non-important areas in the image. Subsequently, we clip the CAM values to the range [0.3, 0.7] and normalize them to obtain the probability matrix P. We sample according to the P to obtain the coordinate (x, y) , and then set the $k \times k$ area around (x, y) to be 1 and the remaining areas to be 0 to obtain mask m . Here, m has the same shape as \tilde{x}_t . This approach disperses more adversarial features in non-important areas and less in important areas of adversarial examples, improving the natural visual effect of adversarial examples.

At each denoising step t , we combine x_t and \tilde{x}_t as the following:

$$\hat{x}_t = m \odot x_t + (1 - m) \odot \tilde{x}_t \quad (9)$$

where \odot refers to Hadamard Product. Afterwards, we can obtain new score by integrating $\epsilon_{\theta}(\hat{x}_t)$ with the estimated gradient information and then use $\tilde{x}_{t-1} = -\sqrt{1 - \bar{\alpha}_t} \times \text{score}$ for sampling.

We provide a complete algorithmic overview of AdvDiffVLM in Algorithm 1. Finally, we find that new adversarial examples obtained by taking the generated adversarial examples as x_0 , and then iterating N times in this way has stronger transferability as well as greater robustness against adversarial defense methods. We refer to this approach as AdvDiffVLM+ and set $N = 3$.

4.4 Differences From AdvDiffuser

Both our method and AdvDiffuser [5] produce unrestricted adversarial examples using the diffusion model. Here, we discuss the distinctions between them, highlighting our contributions.

Tasks of varying difficulty levels: AdvDiffuser is oriented towards classification models, while our research targets the more intricate Vision-Language Models (VLMs). Initially, within the realm of classification tasks, each image is associated with a singular label. Conversely, in the image-to-text tasks, images may be linked to numerous text descriptions. When faced with an attack targeting a singular description, VLMs have the capability to generate an alternate description, thereby neutralizing the attack’s effectiveness. As a result, our task presents a greater challenge.

Different theoretical foundations: AdvDiffuser posits that PGD can introduce adversarial noise. It begins with Gaussian noise, subsequently incorporating high-frequency adversarial perturbations into the latent image in a sequential manner. Given that the diffusion model’s inverse process inherently constitutes a denoising procedure, it necessitates numerous iterations to introduce sufficient perturbations, leading to heavy computation. In contrast, our method derives from score matching, where we employ CLIP to estimate gradient, subsequently altering the score rather than adding it into latent image. Through score matching, the adversarial gradient can be perfectly integrated into the reverse generation process without being weakened. Furthermore, our approach obviates the need for initiating with Gaussian noise, initially introducing noise to \mathbf{x} through t^* steps, followed by the application of adversarial gradient to modify score, thereby facilitating more efficient generation of adversarial examples. See Appendix 3.3 for visual illustrations.

Distinct schemes of GradCAM utilization: The GradCAM mask utilized by AdvDiffuser leads to restricted modification of crucial image areas, rendering it inadequate for image-based attacks. Addressing this issue, we have introduced the GradCAM-guided Mask. Contrary to utilizing GradCAM results directly as a mask, we employ them as a directive to generate the mask further. This not only guarantees a likelihood of modification across all image areas but also secures minimal alteration of significant areas, striking a balance between image quality and attack ability.

5 EXPERIMENTS

5.1 Experimental Setup

Datasets and Victim VLMs: Following [6], we use NeurIPS’17 adversarial competition dataset, compatible with ImageNet, for all the experiments. Else, we select 1,000 text descriptions from the captions of the MS-COCO dataset as our adversarial target texts and then use Stable Diffusion [21] generate 1,000 adversarial targeted images. For the victim VLMs, SOTA open-source models are evaluated, including MiniGPT-4 [33], LLaVA [14], UniDiffuser [2],

Table 1: Comparison with existing SOTA attack methods, where the best result is bolded, and the second-best result is underlined. Note that we use four versions of the CLIP visual encoder, including Resnet50, Resnet101, ViT-B/16 and ViT-B/32, as surrogate models. Besides, AdvDiffVLM_{single} means using a single ViT-B/32 to calculate the loss, AdvDiffVLM_{ens} means using a simple ensemble strategy, and AdvDiffVLM_{nomask} means not using GradCAM-guided Mask. Since Unidiffuser uses ViT-B/32 as the visual encoder, it is a gray box scenario, which we indicate with *. The shaded parts represent our two proposed methods.

| | Unidiffuser* | | BLIP | | BLIP2 | | MiniGPT-4 | | LLaVA | | Img2LLM | | Time(s) |
|---------------------------------|-----------------------|-------|-----------------------|------------|-----------------------|------------|-----------------------|------------|-----------------------|------------|-----------------------|------------|-----------|
| | CLIP _{tar} ↑ | ASR ↑ | CLIP _{tar} ↑ | ASR ↑ | CLIP _{tar} ↑ | ASR ↑ | CLIP _{tar} ↑ | ASR ↑ | CLIP _{tar} ↑ | ASR ↑ | CLIP _{tar} ↑ | ASR ↑ | |
| Original | 0.4770 | 0% | 0.5190 | 0% | 0.4931 | 0% | 0.4902 | 0% | 0.5190 | 0% | 0.5288 | 0% | / |
| Ens | 0.7353 | 99% | 0.5322 | 4% | 0.5085 | 1% | 0.4980 | 2% | 0.5366 | 3% | 0.5297 | 4% | 69 |
| SVRE | 0.7231 | 100% | 0.5410 | 5% | 0.5190 | 2% | 0.5107 | 2% | 0.5385 | 4% | 0.5292 | 4% | 125 |
| CWA | 0.7568 | 100% | 0.5415 | 9% | 0.5249 | 5% | 0.5211 | 4% | 0.5493 | 7% | 0.5346 | 5% | 101 |
| SSA-Ens | 0.7275 | 100% | 0.5991 | 31% | 0.5539 | 9% | 0.5175 | 10% | 0.6098 | 37% | 0.5629 | 19% | 879 |
| SSA-SVRE | 0.7217 | 100% | 0.6002 | 34% | 0.5776 | 18% | 0.5395 | 16% | 0.6005 | 40% | 0.5625 | 18% | 1012 |
| SSA-CWA | 0.7485 | 100% | 0.6074 | 36% | 0.5888 | 23% | 0.5407 | 20% | 0.6152 | 41% | 0.5634 | 20% | 1225 |
| SIA-Ens | 0.7377 | 100% | 0.7001 | 79% | 0.5656 | 50% | 0.5305 | 40% | <u>0.7158</u> | 85% | 0.6337 | 27% | 483 |
| SIA-SVRE | 0.7302 | 100% | <u>0.7014</u> | <u>81%</u> | 0.5802 | 50% | 0.5482 | 46% | 0.7122 | <u>88%</u> | 0.6305 | <u>35%</u> | 596 |
| SIA-CWA | <u>0.7498</u> | 100% | 0.7059 | 89% | 0.5835 | <u>56%</u> | 0.5510 | 48% | 0.7194 | 90% | 0.6401 | 40% | 732 |
| AdvDiffuser _{ens} | 0.6774 | 86% | 0.5504 | 24% | 0.5396 | 8% | 0.5371 | 8% | 0.5507 | 25% | 0.5395 | 11% | 574 |
| AdvDiffuser _{adaptive} | 0.6932 | 88% | 0.5631 | 29% | 0.5424 | 10% | 0.5391 | 9% | 0.5595 | 27% | 0.5502 | 14% | 602 |
| AdvDiffVLM _{single} | 0.6977 | 95% | 0.5322 | 3% | 0.5073 | 1% | 0.5022 | 2% | 0.5332 | 6% | 0.5351 | 3% | 13 |
| AdvDiffVLM _{ens} | 0.7050 | 100% | 0.6044 | 46% | 0.5708 | 34% | 0.5402 | 31% | 0.6035 | 53% | 0.5847 | 20% | 15 |
| AdvDiffVLM _{nomask} | 0.7416 | 100% | 0.6484 | 59% | 0.6357 | 55% | 0.6019 | 50% | 0.6552 | 73% | 0.6105 | 32% | 14 |
| AdvDiffVLM | 0.7329 | 100% | 0.6402 | 52% | 0.6137 | 50% | 0.5814 | 46% | 0.6426 | 70% | 0.6032 | 28% | 15 |
| AdvDiffVLM+ | 0.7398 | 100% | 0.6511 | 61% | <u>0.6314</u> | 58% | 0.6035 | 52% | 0.6570 | 77% | <u>0.6338</u> | <u>35%</u> | 42 |

BLIP [13], BLIP2 [12] and Img2LLM [8]. Among them, Unidiffuser is a gray-box model, and the others are black-box models.

Baselines: We compare with AdvDiffuser [5] and other SOTA transfer-based attackers described in Section 3.2. Since AdvDiffuser is used for classification models, we use cosine similarity loss instead of classification loss for adversarial attacks on VLMs. For a fair comparison, we implement the ensemble version of AdvDiffuser, including simple ensemble and adaptive ensemble, which are denoted as AdvDiffuser_{ens}, AdvDiffuser_{adaptive} respectively.

Evaluation Metrics: Following [31], we adopt CLIP score between the generated responses from victim models and predefined targeted texts, as computed by ViT-B/32 text encoder, referred as CLIP_{tar}. We adopt the method of calculating the attack success rate (ASR) in [6], positing that an attack is deemed successful solely if the image description includes the target semantic main object. In order to measure the quality of adversarial examples and the perceptibility of applied perturbations, we use four evaluation metrics: SSIM [28], FID [9], LPIPS [30] and BRISQUE [18].

Implementation Details: Since our adversarial diffusion sampling does not require additional training to the original diffusion model, we use the pre-trained diffusion model in our experiment. We adapt LDM [21] with DDIM sampler [24] (the number of diffusion steps $T = 200$). For surrogate models, we select four versions of CLIP [20], namely Resnet50, Resnet101, ViT-B/16 and ViT-B/32. For other hyperparameters, we use $s = 35$, $\delta = 0.0025$, $t^* = 0.2$, $k = 8$ and $\tau = 2$, where $t^* = 0.2$ means adding noise to \mathbf{x} in $0.2 \times T$ steps and then performing the reverse process. All the experiments are conducted on a Tesla A100 GPU with 40GB memory.

The detailed introduction to the victim models, baselines, and evaluation metrics are given in Appendix 4.

5.2 Comparison Results

Attack Comparison. To validate the effectiveness of AdvDiffVLM, we first evaluate the transferability of adversarial examples generated by AdvDiffVLM and baselines on various VLMs. As shown in Table 1, all methods exhibit favorable attack results in gray box scenarios. Within the transfer attack scenario, our method yields performance comparable to the SOTA method SIA-CWA. Specifically, our method surpasses SIA-CWA in BLIP2 and MiniGPT-4, marking improvements in the CLIP_{tar} by 0.0479 and 0.0525, respectively. Although in the cases of BLIP and LLaVA, SIA-CWA exceeds the performance of our approach, it is particularly important to note that our method requires less than *one-tenth of the time* compared to SIA for generating adversarial examples, which makes our method more practical in practice. We will analyze efficiency issues further in Appendix 5.2. Additionally, it has been observed that AdvDiffuser exhibits suboptimal performance in challenging attack scenarios, particularly against VLMs. This is attributed to its direct application of GradCAM as the mask, which restricts the modifiable area for adversarial examples in demanding tasks, thereby diminishing attack effectiveness. Simultaneously, AdvDiffuser employs high-frequency adversarial noise to alter semantics. This adversarial noise, being inherently fragile, is significantly mitigated during the diffusion model’s reverse process, further diminishing its attack potential on complex tasks. These observations validate the advantages of our GradCAM-guided Mask and score matching idea.

Defense. We adopt SOTA defense method, *i.e.* DiffPure [19], to validate the robustness of our proposed method. The results are reported in Table 2. It can be found that our method outperforms baselines in both gray-box and black-box settings. For example, on Unidiffuser, for CLIP_{tar} score, our method is 0.0689 higher than

Table 2: Defense results with DiffPure. The setting are the same as Table 1 except the adversarial examples are purified by DiffPure. In this table, $CLIP_{tar}$ evaluates the similarity between the purified examples and the target texts.

| | Unidiffuser* | | BLIP | | BLIP2 | | MiniGPT-4 | | LLaVA | | Img2LLM | |
|---------------------------------|-----------------------|----------------|-----------------------|----------------|-----------------------|----------------|-----------------------|----------------|-----------------------|----------------|-----------------------|----------------|
| | $CLIP_{tar} \uparrow$ | ASR \uparrow | $CLIP_{tar} \uparrow$ | ASR \uparrow | $CLIP_{tar} \uparrow$ | ASR \uparrow | $CLIP_{tar} \uparrow$ | ASR \uparrow | $CLIP_{tar} \uparrow$ | ASR \uparrow | $CLIP_{tar} \uparrow$ | ASR \uparrow |
| Original | 0.4802 | 0% | 0.5124 | 0% | 0.4924 | 0% | 0.4831 | 0% | 0.5253 | 0% | 0.5302 | 0% |
| Ens | 0.4833 | 0% | 0.5149 | 0% | 0.4929 | 0% | 0.4840 | 0% | 0.5263 | 0% | 0.5332 | 0% |
| SVRE | 0.4846 | 0% | 0.5224 | 1% | 0.4953 | 0% | 0.4852 | 0% | 0.5264 | 0% | 0.5312 | 0% |
| CWA | 0.4873 | 2% | 0.5268 | 1% | 0.4973 | 0% | 0.4901 | 1% | 0.5272 | 1% | 0.5307 | 0% |
| SSA-Ens | 0.4914 | 1% | 0.5292 | 0% | 0.5024 | 0% | 0.4996 | 0% | 0.5280 | 1% | 0.5322 | 0% |
| SSA-SVRE | 0.4899 | 2% | 0.5285 | 0% | 0.4984 | 0% | 0.4988 | 0% | 0.5273 | 1% | 0.5356 | 0% |
| SSA-CWA | 0.4868 | 2% | 0.5312 | 1% | 0.4997 | 0% | 0.4997 | 2% | 0.5283 | 3% | 0.5367 | 1% |
| SIA-Ens | 0.4921 | 3% | 0.5351 | 1% | 0.5068 | 1% | 0.5009 | 1% | 0.5356 | 2% | 0.5372 | 2% |
| SIA-SVRE | 0.4930 | 3% | 0.5355 | 1% | 0.5012 | 2% | 0.5011 | 2% | 0.5349 | 4% | 0.5380 | 2% |
| SIA-CWA | 0.4942 | 5% | 0.5379 | 2% | 0.5099 | 3% | 0.5025 | 2% | 0.5360 | 4% | 0.5388 | 2% |
| AdvDiffuser _{ens} | 0.4920 | 4% | 0.5201 | 4% | 0.4933 | 2% | 0.4906 | 2% | 0.5325 | 3% | 0.5310 | 2% |
| AdvDiffuser _{adaptive} | 0.4922 | 4% | 0.5227 | 4% | 0.5001 | 3% | 0.5001 | 3% | 0.5336 | 3% | 0.5325 | 2% |
| AdvDiffVLM _{single} | 0.4902 | 1% | 0.5322 | 0% | 0.4995 | 0% | 0.4904 | 0% | 0.5327 | 1% | 0.5258 | 0% |
| AdvDiffVLM _{ens} | 0.5129 | 12% | 0.5515 | 7% | 0.5102 | 3% | 0.5096 | 4% | 0.5444 | 8% | 0.5419 | 2% |
| AdvDiffVLM _{nomask} | <u>0.5407</u> | <u>15%</u> | <u>0.5762</u> | <u>13%</u> | 0.5348 | 6% | <u>0.5273</u> | <u>7%</u> | <u>0.5590</u> | <u>14%</u> | <u>0.5493</u> | <u>6%</u> |
| AdvDiffVLM | 0.5302 | <u>15%</u> | 0.5707 | 11% | 0.5226 | <u>5%</u> | 0.5184 | 6% | 0.5551 | 11% | 0.5450 | 4% |
| AdvDiffVLM+ | 0.5631 | 18% | 0.5832 | 15% | <u>0.5315</u> | 6% | 0.5309 | 8% | 0.5617 | 15% | 0.5531 | 7% |

Table 3: Quality comparison of adversarial examples under four evaluation metrics. The best result is bolded, and the second-best result is underlined.

| Method | SSIM \uparrow | LPIPS \downarrow | FID \downarrow | BRISQUE \downarrow |
|---------------------------------|-----------------|--------------------|------------------|----------------------|
| SSA-Ens | 0.6687 | 0.3320 | 110.5 | 66.89 |
| SSA-SVRE | 0.6610 | 0.3325 | 112.6 | 70.05 |
| SSA-CWA | 0.6545 | 0.3673 | 123.4 | 67.67 |
| SIA-Ens | 0.6925 | 0.2990 | 117.3 | 55.61 |
| SIA-SVRE | 0.6920 | 0.3042 | 120.0 | 57.42 |
| SIA-CWA | 0.6892 | 0.3306 | 125.3 | 56.02 |
| AdvDiffuser _{ens} | 0.6520 | 0.3074 | 115.5 | 14.61 |
| AdvDiffuser _{adaptive} | 0.6471 | 0.3096 | 126.7 | <u>15.32</u> |
| AdvDiffVLM _{ens} | 0.6721 | 0.1834 | 90.4 | 17.48 |
| AdvDiffVLM _{nomask} | <u>0.7129</u> | 0.2687 | 111.9 | 16.92 |
| AdvDiffVLM | 0.7188 | <u>0.2358</u> | <u>96.1</u> | 16.80 |
| AdvDiffVLM+ | 0.7008 | 0.2577 | 104.4 | 19.17 |

SIA-CWA. On BLIP, for $CLIP_{tar}$ score, our method is 0.0453 higher than SIA-CWA. These experimental results show that our method is more robust than baselines in evading DiffPure defense method. Additional defense results are provided in Appendix 5.3.

Image Quality Comparison. We evaluate the image quality of the generated adversarial examples using four evaluation metrics: SSIM, FID, LPIPS, and BRISQUE. As shown in Table 3, compared to transfer-based attacks and AdvDiffuser, the adversarial examples generated by our method exhibit superior image quality. Additionally, we find that for the BRISQUE metric, AdvDiffuser is better than our method. However, as shown in Figure 4, the perturbation introduced by our method is semantic, while AdvDiffuser significantly alters the non-salient area, resulting in poor visual effects.

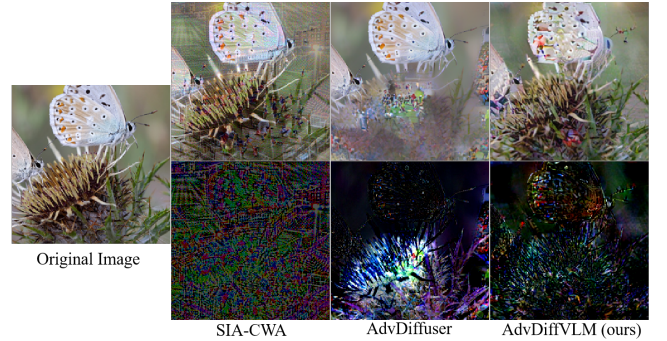


Figure 4: Visualization of adversarial perturbations generated by different attack methods. Note that the first row represents adversarial examples, and the second row represents adversarial perturbations. We choose SIA-CWA and AdvDiffuser_{adaptive} as representatives of baselines. We amplify the perturbation values for better visualization.



Figure 5: Visualization of the attack results of AdvDiffVLM on BLIP. We show the adversarial target text above the image, and display the image caption results of original image and adversarial example below the image.

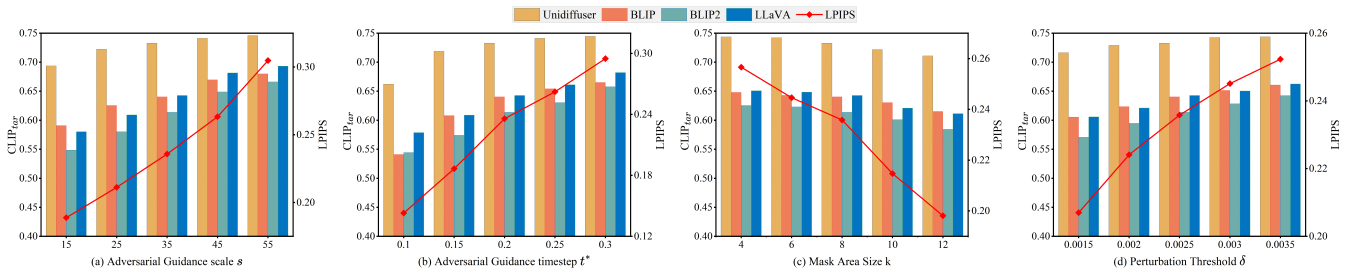


Figure 6: Ablation study of the impact of various parameters in AdvDiffVLM. We adopt the $CLIP_{tar}$ and LPIPS scores to show the impact of transferability and image quality with four VLMs. A higher $CLIP_{tar}$ value indicates better performance, whereas a lower LPIPS value signifies better results. We only vary one of the hyperparameters at a time, and then fix the other three hyperparameters to the preset values shown in Section 5.1. Note: the results of $CLIP_{tar}$ are presented using bar graphs, while LPIPS results are depicted using dot-line graphs.

Else, SIA-CWA introduces irregular high-frequency noise, which can be easily found. More visualization results in Appendix 5.4.

In summary, our method can generate adversarial examples with transferability comparable to the SOTA transfer-based attack SIA-CWA with a speedup of over 10X. More importantly, the generated adversarial examples have better image quality and exhibit better robustness to adversarial defense methods.

5.3 Visualize Results

We visualize the attack results of our method on VLMs. As shown in Figure 5, our method successfully induces black-box VLMs to output adversarial target semantics. For example, for the adversarial target text "This little girl is taking tennis lessons to learn how to play", we successfully make BLIP output "a little girl play with a teddy bear and a tennis ball", while the original response to the image is "an adult black and write panda bear". See Appendix 5.5 for more visualization results.

5.4 Attack results on commercial VLMs

Our method can successfully attack commercial VLMs such as GPT-4V in black-box scenarios. For example, as shown in Figure 7, we can successfully attack the hosted GPT-4V API. Specifically, for the adversarial target text "A bird standing on top of a beach next to water", we successfully make GPT-4V output a similar target response, while the semantics of the original image is a dog. Additional visualize and quantitative results of attacks on GPT-4V and other commercial VLMs, such as Google’s Gemini, Microsoft’s Copilot, and Baidu’s ERNIE Bot, are detailed in Appendix 5.6.

5.5 Ablation Experiments

To further understand the effectiveness of the proposed method, we first discuss the role of each module.

Are adaptive ensemble method beneficial for boosting the transferability? First, as shown in Tables 1 and 2, using the ensemble method has improved performance in terms of transferability and robustness compared to using a single loss. Second, we observe that the adaptive method has further improved performance compared with simple ensemble. For example, in Table 1, on BLIP, for the $CLIP_{tar}$ score, the ensemble method improved by 0.0722 compared with the single loss, and after using the adaptive method, it

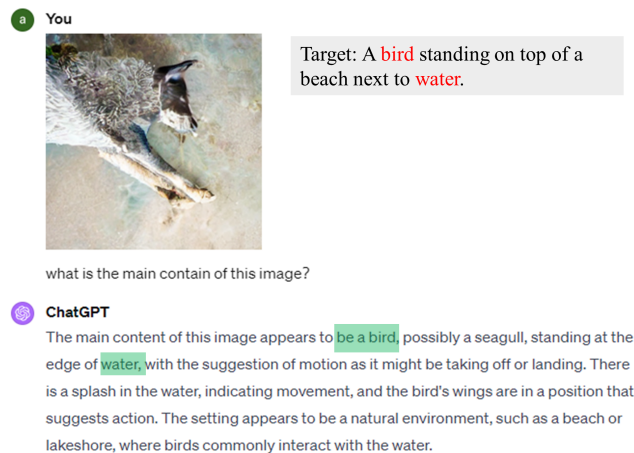


Figure 7: Screenshots of successful attacks against GPT-4V API’s image description. We give the adversarial target text on the right side of the image. Else, we mark the main objects of the adversarial target in red and the main objects in the GPT-4V response in green.

further improved by 0.0358. This proves that the adaptive ensemble method can help improve transferability.

Does GradCAM-guided Mask help trade-off image quality and transferability? As shown in Table 1, the use of GradCAM-guided Mask results in a slight decrease in the transferability of adversarial examples. For example, on BLIP, after using GradCAM-guided Mask, the $CLIP_{tar}$ score decrease by 0.0082. However, as indicated in Table 3, the application of GradCAM-guided Mask leads to an improvement in the quality of adversarial examples. This highlights that GradCAM-guided Mask assists in balancing the visual effects and attack capabilities of adversarial examples.

The impacts of parameters. We now discuss the impacts of AdvDiffVLM parameters (including the s , t^* , k , and δ) in Figure 6 by conducting tests on Unidiffuser, BLIP, BLIP2, and LLaVA. It is evident that all parameters influence the trade-off between transferability and image quality. Increasing values for parameters s , t^* , and δ enhance transferability but diminish the visual quality of adversarial examples. This is because larger values for these parameters result in a greater perturbation, allowing for the embedding of more adversarial semantics into the image. Conversely, increasing

the value of k produces adversarial examples with improved visual effects but reduces transferability. The reason is that larger values of k result in a larger generated mask, making it more challenging to modify the important areas in the image. To achieve an optimal trade-off between transferability and image quality, we empirically select $s = 35$, $t^* = 0.2$, $k = 8$ and $\delta = 0.0025$.

6 CONCLUSION

In this work, we propose AdvDiffVLM, an unrestricted adversarial example generation method for VLMs. We designed the Adaptive Ensemble Gradient Estimation based on the idea of score matching. It embeds target semantics into adversarial examples with a 10x to 30x boost in speed over existing systems. At the same time, in order to achieve a trade-off between adversarial example quality and attack capabilities, we propose the GradCAM-guided Mask module. Extensive experiments demonstrate that AdvDiffVLM can efficiently generate adversarial examples with transferability compared to current SOTA transfer-based attacks. Simultaneously, these adversarial examples exhibit superior image quality and greater robustness to adversarial defense methods.

REFERENCES

- [1] Nayyer Aafaq, Naveed Akhtar, Wei Liu, Mubarak Shah, and Ajmal Mian. 2022. Language model agnostic gray-box adversarial attack on image captioning. *IEEE Transactions on Information Forensics and Security* 18 (2022), 626–638.
- [2] Fan Bao, Shen Nie, Kaiwen Xue, Chongxuan Li, Shi Pu, Yaole Wang, Gang Yue, Yue Cao, Hang Su, and Jun Zhu. 2023. One transformer fits all distributions in multi-modal diffusion at scale. In *International Conference on Machine Learning*. 1692–1717.
- [3] Zikui Cai, Yaoteng Tan, and M Salman Asif. 2023. Ensemble-based blackbox attacks on dense prediction. In *Proceedings of the IEEE/CVF Conference on Computer Vision and Pattern Recognition*. 4045–4055.
- [4] Huanran Chen, Yichi Zhang, Yinpeng Dong, and Jun Zhu. 2024. Rethinking Model Ensemble in Transfer-based Adversarial Attacks. In *The Twelfth International Conference on Learning Representations*. <https://openreview.net/forum?id=AcJrSoArlh>
- [5] Xinquan Chen, Xitong Gao, Juanjuan Zhao, Kejiang Ye, and Cheng-Zhong Xu. 2023. Advdiffuser: Natural adversarial example synthesis with diffusion models. In *Proceedings of the IEEE/CVF International Conference on Computer Vision*. 4562–4572.
- [6] Yinpeng Dong, Huanran Chen, Jiawei Chen, Zhengwei Fang, Xiao Yang, Yichi Zhang, Yu Tian, Hang Su, and Jun Zhu. 2023. How robust is Google’s bard to adversarial image attacks? *arXiv preprint arXiv:2309.11751* (2023).
- [7] Yinpeng Dong, Fangzhou Liao, Tianyu Pang, Hang Su, Jun Zhu, Xiaolin Hu, and Jianguo Li. 2018. Boosting adversarial attacks with momentum. In *Proceedings of the IEEE Conference on Computer Vision and Pattern Recognition*. 9185–9193.
- [8] Jiaxian Guo, Junnan Li, Dongxu Li, Anthony Meng Huat Tiong, Boyang Li, Dacheng Tao, and Steven Hoi. 2023. From images to textual prompts: Zero-shot visual question answering with frozen large language models. In *Proceedings of the IEEE/CVF Conference on Computer Vision and Pattern Recognition*. 10867–10877.
- [9] Martin Heusel, Hubert Ramsauer, Thomas Unterthiner, Bernhard Nessler, and Sepp Hochreiter. 2017. Gans trained by a two time-scale update rule converge to a local nash equilibrium. In *Advances in Neural Information Processing Systems*, Vol. 30. 6629–6640.
- [10] Jonathan Ho, Ajay Jain, and Pieter Abbeel. 2020. Denoising diffusion probabilistic models. *Advances in Neural Information Processing Systems* 33 (2020), 6840–6851.
- [11] Raz Lapid and Moshe Sipper. 2023. I see dead people: Gray-box adversarial attack on image-to-text models. In *Proceedings of the European Conference on Machine Learning and Principles and Practice of Knowledge Discovery in Databases*.
- [12] Junnan Li, Dongxu Li, Silvio Savarese, and Steven Hoi. 2023. BLIP-2: Bootstrapping language-image pre-training with frozen image encoders and large language models. In *International Conference on Machine Learning*. 1–13.
- [13] Junnan Li, Dongxu Li, Caiming Xiong, and Steven Hoi. 2022. BLIP: Bootstrapping language-image pre-training for unified vision-language understanding and generation. In *International Conference on Machine Learning*. PMLR, 12888–12900.
- [14] Haotian Liu, Chunyuan Li, Qingyang Wu, and Yong Jae Lee. 2023. Visual instruction tuning. In *Thirty-seventh Conference on Neural Information Processing Systems*. <https://openreview.net/forum?id=w0H2xGHlkw>
- [15] Yuyang Long, Qilong Zhang, Boheng Zeng, Lianli Gao, Xianglong Liu, Jian Zhang, and Jingkuan Song. 2022. Frequency domain model augmentation for adversarial attack. In *European Conference on Computer Vision*. Springer, 549–566.
- [16] Calvin Luo. 2022. Understanding diffusion models: A unified perspective. *arXiv preprint arXiv:2208.11970* (2022).
- [17] Aleksander Madry, Aleksandar Makelov, Ludwig Schmidt, Dimitris Tsipras, and Adrian Vladu. 2018. Towards deep learning models resistant to adversarial attacks. In *International Conference on Learning Representations*. <https://openreview.net/forum?id=rJzIBfZAb>
- [18] Anish Mittal, Anush K Moorthy, and Alan C Bovik. 2011. Blind/referenceless image spatial quality evaluator. In *2011 conference record of the forty fifth asilomar conference on signals, systems and computers (ASILOMAR)*. IEEE, 723–727.
- [19] Weili Nie, Brandon Guo, Yujia Huang, Chaowei Xiao, Arash Vahdat, and Anima Anandkumar. 2022. Diffusion models for adversarial purification. In *International Conference on Machine Learning*. 1–23.
- [20] Alec Radford, Jong Wook Kim, Chris Hallacy, Aditya Ramesh, Gabriel Goh, Sandhini Agarwal, Girish Sastry, Amanda Askell, Pamela Mishkin, Jack Clark, et al. 2021. Learning transferable visual models from natural language supervision. In *International Conference on Machine Learning*. PMLR, 8748–8763.
- [21] Robin Rombach, Andreas Blattmann, Dominik Lorenz, Patrick Esser, and Björn Ommer. 2022. High-resolution image synthesis with latent diffusion models. In *Proceedings of the IEEE/CVF Conference on Computer Vision and Pattern Recognition*. 10684–10695.
- [22] Ramprasaath R Selvaraju, Michael Cogswell, Abhishek Das, Ramakrishna Vedantam, Devi Parikh, and Dhruv Batra. 2017. Grad-cam: Visual explanations from deep networks via gradient-based localization. In *Proceedings of the IEEE International Conference on Computer Vision*. 618–626.
- [23] Ali Shahin Shamsabadi, Ricardo Sanchez-Matilla, and Andrea Cavallaro. 2020. Colorfool: Semantic adversarial colorization. In *Proceedings of the IEEE/CVF Conference on Computer Vision and Pattern Recognition*. 1151–1160.
- [24] Jiaming Song, Chenlin Meng, and Stefano Ermon. 2021. Denoising diffusion implicit models. In *International Conference on Learning Representations*. <https://openreview.net/forum?id=St1giarCHLP>
- [25] Yang Song, Rui Shu, Nate Kushman, and Stefano Ermon. 2018. Constructing unrestricted adversarial examples with generative models. In *Advances in Neural Information Processing Systems*, Vol. 31. 8322–8333.
- [26] Yang Song, Jascha Sohl-Dickstein, Diederik P Kingma, Abhishek Kumar, Stefano Ermon, and Ben Poole. 2020. Score-based generative modeling through stochastic differential equations. *arXiv preprint arXiv:2011.13456* (2020).
- [27] Xiaosen Wang, Zeliang Zhang, and Jianping Zhang. 2023. Structure invariant transformation for better adversarial transferability. In *Proceedings of the IEEE/CVF International Conference on Computer Vision*. 4607–4619.
- [28] Zhou Wang, Alan C Bovik, Hamid R Sheikh, and Eero P Simoncelli. 2004. Image quality assessment: from error visibility to structural similarity. *IEEE transactions on image processing* 13, 4 (2004), 600–612.
- [29] Yifeng Xiong, Jiadong Lin, Min Zhang, John E Hopcroft, and Kun He. 2022. Stochastic variance reduced ensemble adversarial attack for boosting the adversarial transferability. In *Proceedings of the IEEE/CVF Conference on Computer Vision and Pattern Recognition*. 14983–14992.
- [30] Richard Zhang, Phillip Isola, Alexei A Efros, Eli Shechtman, and Oliver Wang. 2018. The unreasonable effectiveness of deep features as a perceptual metric. In *Proceedings of the IEEE Conference on Computer Vision and Pattern Recognition*. 586–595.
- [31] Yunqing Zhao, Tianyu Pang, Chao Du, Xiao Yang, Chongxuan Li, Ngai-Man Cheung, and Min Lin. 2023. On evaluating adversarial robustness of large vision-language models. In *Thirty-seventh Conference on Neural Information Processing Systems*.
- [32] Zhengli Zhao, Dheeru Dua, and Sameer Singh. 2018. Generating natural adversarial examples. In *International Conference on Learning Representations*. <https://openreview.net/forum?id=H1BLjgZCb>
- [33] Deyao Zhu, Jun Chen, Xiaoqian Shen, Xiang Li, and Mohamed Elhoseiny. 2023. Mini-gpt-4: Enhancing vision-language understanding with advanced large language models. *arXiv preprint arXiv:2304.10592* (2023).